

Mathematical Analysis of an Euler Spring Vibration Isolator.

J. Winterflood, T.A. Barber, D. G. Blair

Department of Physics, University of Western Australia, Perth 6907, Australia.

A new suspension technique uses flat springs in Euler buckling mode. This numerical analysis of the basic lever constrained configuration identifies the effect of the main geometrical parameters, and suitable values for obtaining the most useful force-displacement characteristic. The theory is shown to agree well with experimental measurements.

1 Introduction

A new suspension technique was presented recently[2] which minimises the mass of spring material required for suspension against a constant force such as gravity. This has major advantages in reducing the isolation bypassing effect of internal resonances, and the technique also avoids the large pre-loading strain which must generally be established. The technique primarily involves using the post-critical elastic buckling properties of a longitudinally compressed column or spring. Elastic buckling is often analysed in the literature, but almost always in order for unstable conditions to be avoided - very rarely in order to make use of its unusual characteristics. An excellent source of theory together with extensive experimental comparison of the general post-buckling behaviour of various structures is given by Britvec [1]. This paper focuses on one particular structure which we have developed for vibration isolation and analyses the effect of various configuration parameters on the final force-displacement and frequency-displacement relationships obtained.

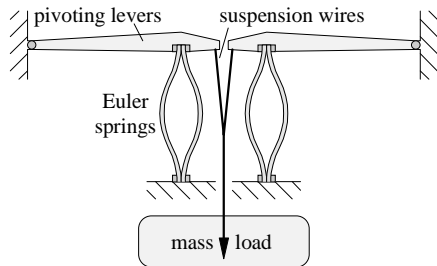


FIGURE 1. The balanced form of the geometry to be analysed.

A typical vibration isolation structure employing Euler springs is shown in figure 1 in which the suspended mass is supported by spring elements loaded in compression so that they just start to buckle elastically. A pivoted lever is a simple way to keep the motion planar and prevent lateral instability. Two are used in figure 1 to form a balanced arrangement to avoid cross-coupling from vertical to other modes of motion. A result of using the pivoted lever mounting is that one end of the clamped flexures is constrained to rotate through a certain angle as the load displaces and the springs compress. This paper analyses the effect that this rotation has on the resulting force-displacement characteristic and how it changes with the main

parameters such as lever arm radius and spring launching angles.

2 Geometrical Model

In order to analyse the performance of the structure shown in figure 1, we consider just the right hand lever and only show the flexure which is deflecting towards the pivot. Figure 2 shows this essential geometry drawn so that the flexure is approximately horizontal. Lengths have been normalised by taking the length of the flexure to be unity so that all lengths (such as the radius R of the lever) are given as a ratio to the flexure length. Lever pivoting angles are measured with respect to a reference position where the flexure clamping points would form a right angle with the pivoting centre. The main benefits of this suspension technique are obtained when operated at small spring buckling deflections. For this reason the pivoting angles considered only vary very slightly from this square position. The length D is the length of a straight line between the clamping points on the flexure and this line is used as a reference for various angular measurements. In particular when the flexure is stretched straight so that it lies along this line (ie $D=1$ at maximum clockwise pivot position θ_0) then the launching angles α_F and α_P (typically 0°) that the ends of the flexure are clamped at are measured with respect to this line.

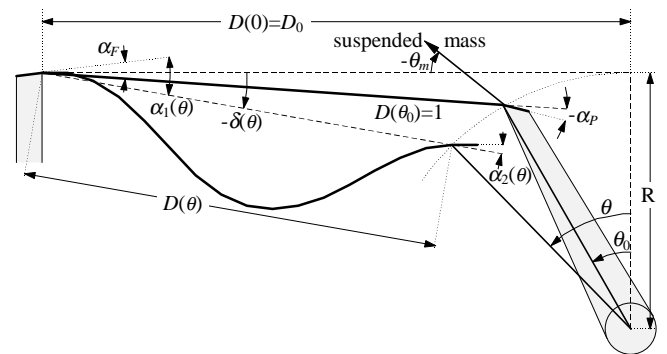


FIGURE 2. Variables for analysis of the geometry.

When the flexure is buckled to form a curve, it can be deflected either towards the pivot (downward as shown) or away from it. With more than one flexure (eg figure 1) deflection can occur in both directions and the force contribution from each direction can be infinitely varied from

one, to both, to the other (eg by varying their thicknesses). A parameter B_P is used to represent the fraction of the force being contributed from the flexure bending towards the pivot.

The main parameters which may be configured in order to obtain desirable system performance are identified in figure 2 and are summarised as follows :-

- R Lever radius (normalised to the flexure length).
- α_F Flex clamp angle at fixed end (w.r.t strip at θ_0)
- α_P Flex clamp angle at pivot end (w.r.t strip at θ_0)
- B_P Force fraction from strip deflecting towards pivot.

Another parameter which may be varied is the attachment angle of the suspended mass θ_m . If the mass is made to pull in a significantly different direction than along the line of the flexure, some sinusoidal non-linearity can be obtained. However this parameter, together with a few other possible variables (for instance θ_0) typically have to be pushed to unlikely values in order to contribute a significant effect. The variables are included in the mathematics for completeness but they are left at zero for the plots and their effect is not explicitly analysed. (The angle of the suspended mass θ_m required to null the basic spring rate is indicated in figure 13b of the earlier paper[2].)

The geometry of the pivoting lever and end clamps determine three boundary conditions applied to the flexures which dictate the two possible stable states that the flexure can take on. These boundary conditions are :-

- D Distance between clamps as ratio to flexure length
- α_1 Left hand clamp angle (w.r.t straight joining line)
- α_2 Right hand clamp angle (w.r.t straight joining line)

Given the previous set of configuration parameters, these three flexure boundary conditions can be found from :-

$$D = R\sqrt{(D_0/R - \sin\theta)^2 + (1 - \cos\theta)^2}$$

$$\alpha_1 = \alpha_F - (\delta(\theta) - \delta(\theta_0))$$

$$\alpha_2 = \alpha_P - (\theta - \theta_0) + (\delta(\theta) - \delta(\theta_0))$$

where $\delta(\theta) = \tan^{-1}[(\cos\theta - 1)/(D_0/R - \sin\theta)]$ (1)

and $D_0/R = \sqrt{1/R^2 - (1 - \cos\theta_0)^2} + \sin\theta_0$

3 Euler Strip Analysis

Consider the thin flat strip of spring material, which in an unstressed state is flat, but is clamped at both ends and has a longitudinal compressive force applied so that it is kept in a buckled state with two points of inflection along its length. The shape that such a strip assumes once clear of the clamps is called an *elastica* and the parametric equations describing

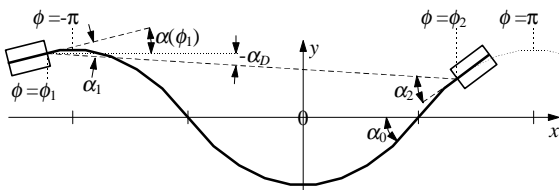


FIGURE 3. Flexure strip boundary conditions.

it make use of elliptic integrals of the first $F(k, \phi)$ and second $E(k, \phi)$ kind where we follow [3] and use k as the modulus and ϕ as the amplitude.

Figure 3 shows this curve positioned on its x -axis which passes through the points of inflection on the strip, and a y -axis through a point of maximum curvature. ϕ becomes the parametric variable which defines points along the curve and x and y coordinates are given by the equations :-

$$x = c(2E(k, \phi) - F(k, \phi))$$

$$y = B 2ck \cos(\phi) \quad (2)$$

where $B=-1$ in equation (2) gives the downward bending solution and $B=+1$ would give an upward arching solution. The curve in figure 3 has ϕ ranging from $\phi_1 \approx -(10\pi/9)$ on the left to $\phi_2 \approx (2\pi/3)$ on the right. The value of c is determined by the flexure's modulus of elasticity E , its moment of inertia I and the compressive force F_x applied along its x -axis :-

$$c = \sqrt{EI/F_x} \quad (3)$$

The modulus k indicates the curvedness of the flexure and is related to the maximum angle α_0 occurring between the elastica and the x -axis. Since α_0 is easier to visualise, we use it to specify the curvedness and k is found from it by :-

$$k = \sin(\alpha_0/2)$$

The angle $\alpha(\phi)$ at any point along the elastica is given by :-

$$\alpha(\phi) = 2 \sin^{-1}(k \sin \phi)$$

The arc length L along the flexure between ϕ_1 and ϕ_2 is :-

$$L = 1 = c(F(k, \phi_2) - F(k, \phi_1))$$

Using these equations, it is easiest to generate a particular elastica given values for :-

- α_0 maximum angle of flexure w.r.t x -axis of elliptic
- ϕ_1 left end termination of incomplete elliptic
- ϕ_2 right end termination of incomplete elliptic
- B Bending direction (+1 = up, -1 = down as figure 3)

Given this set of shape defining values, the flexure boundary conditions (D, α_1, α_2) can be found by the following calculation steps :-

$$k = \sin(\alpha_0/2)$$

$$c = 1/(F(k, \phi_2) - F(k, \phi_1)) \quad (4)$$

$$\Delta x = 2c(E(k, \phi_2) - E(k, \phi_1)) - 1$$

$$\Delta y = 2Bck(\cos\phi_2 - \cos\phi_1)$$

$$D = \sqrt{\Delta x^2 + \Delta y^2}$$

$$\alpha_D = \tan^{-1}(\Delta y/\Delta x)$$

$$\alpha_1 = -(\alpha(\phi_1) - \alpha_D)$$

$$\alpha_2 = -(\alpha(\phi_2) - \alpha_D)$$

where $\alpha(\phi) = 2B \sin^{-1}(k \sin \phi)$

The inverse problem of finding $(\alpha_0, \phi_1, \phi_2)$ given (D, α_1, α_2) is solved numerically by an iterative approach such as by using FindRoot[eqns,vars] in Mathematica®[4]. If B_P is non-integral, then two solutions need to be found - one with $B=1$ for the flexure bending upwards and one with $B=-1$ for the

flexure bending down. These two solutions are used in proportion to determine the overall force-displacement characteristic.

4 Obtaining Force vs Displacement

As a by-product of finding values for $(\alpha_0, \phi_1, \phi_2)$ that solves for a given set of (D, α_1, α_2) , we also obtained a value for c (eqn (4)) from which we can obtain a value for the force using equation (3). This longitudinal force appears acting along the curve's x-axis without torque at the inflection points of the flexure (placing a perfect pivot at an inflection point would have no effect). The torque on the lever is this force multiplied by the perpendicular offset to the lever pivot. This torque (added to any torque from the pivot spring rate) can be translated to a force applied in the direction of the suspended mass giving finally the force vs displacement characteristic.

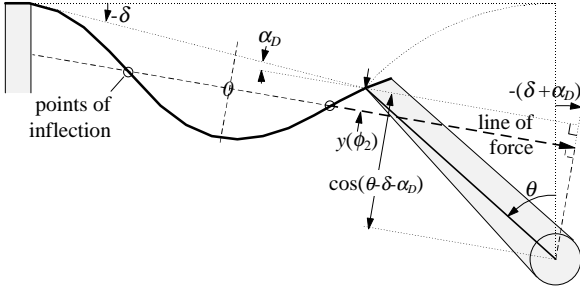


FIGURE 4. Variables for torque and force determination.

If we normalise the force obtainable from equation (3)

$$F_x = EI/c^2$$

to the Euler force of a straight clamped flexure of length $L(=1)$ as it starts to buckle

$$F_e = 4\pi^2 EI/L^2 \quad (5)$$

we obtain the normalised force :-

$$F_n = F_x/F_e = 1/(4\pi^2 c^2)$$

If this force is applied to the lever along the x-axis of the elastica as in figure 4 we obtain a torque T_e on the lever of :-

$$T_e = F_n (R \cos(\theta + \delta - \alpha_D) - y(\phi_2))$$

where δ is found from (1) and $y(\phi_2)$ from (2).

The angular spring rate of pivoting k_p (which includes suspension point pivoting) provides an additional torque $k_p(\theta - \theta_k)$ dependent on the angle θ away from neutral position θ_k . The sum of these two torques appears as a force F_m in the direction of the suspended mass (θ_m in figure 2) :-

$$F_m = (T_e + k_p(\theta - \theta_k)) / (R \cos(\theta - \theta_m)) \quad (6)$$

It is apparent that the suspension point pivoting (ie bending of a suspension wire as the lever rotates) will contribute a much stiffer angular spring-rate, than the lever pivot which is almost unloaded and can be made very thin and flexible. An expression may be obtained for the normalised angular spring-rate k_n from a long round suspension wire strong enough to support the mass m , as a ratio to the angular

spring-rate $k_e = r^2 mg / (2l)$ of an Euler spring length l acting at the same suspension radius r :-

$$k_n = k_p/k_e = l\sqrt{Emg/\pi} / (r^2 \sigma) \quad (7)$$

where E = wire modulus and σ = max wire stress. Using typical values for spring steel wire (loaded to 800MPa) and length = radius = 100mm, this ratio is approx 3% for a suspended mass of 10kg or 10% for 100kg. This poorly defined value is sufficiently small to be neglected in comparison with the Euler spring-rate contribution for qualitative purposes. The force value from (6) is plotted against mass displacement given by :-

$$x_m = R(\sin(\theta - \theta_m) - \sin(\theta_0 - \theta_m))$$

to obtain the following plots. In all of these plots the x-axis displacement and radius R is given as a ratio to the spring blade length, and the force or frequency is given as relative to the value for a perfectly clamped blade under parallel buckling (ie eqn (5) for force or $\omega = (g/(2l))^{1/2}$ for frequency).

5 The Effect of Bending Direction and Lever Radius

Figure 5 indicates how the force-displacement characteristic varies with bending direction and lever radius. When the lever radius is infinite (ie parallel straight-line compression), then the central, almost straight dashed line is obtained. Its gradient (or spring-rate) has a normalised value of 1/2.

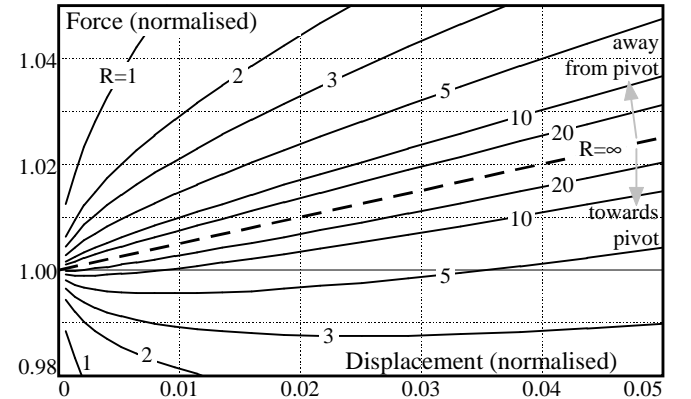


FIGURE 5. Force-displacement dependence on direction and radius.

As the lever radius reduces, the curves for each direction of bending (towards or away from the pivot) separate as negative and positive roots of a square root function (to first order). These curves take the form of approximate parabolas of increasing focal length straddled about the basic Euler spring-rate for parallel compression (the dashed line in the centre). The upper part of the curve corresponds to bending away from the pivot (giving a stiffer spring-rate) while the lower part of the curve corresponds to bending towards the pivot (often giving a negative spring-rate). Varying the proportion of force contributed by springs bending in each direction allow any intermediate curve to be obtained (ie the curves belonging to levers of greater radii). If equal springs are bending in both directions then a force-displacement

relationship graphically indistinguishable from the infinite radius one is obtained.

The significance of these parabolic shaped curves for the isolation technique is that there is no curve that can be selected by radius and spring direction ratio that will give a significantly lower spring-rate than the dashed central line over a reasonable displacement range starting from buckling. Any curve that promises a reasonable range is significantly unstable close to the buckling point. Also if it is desired to only use springs bending towards the pivot (as we tried in [2]), then a rather large radius (between 5 and 10 times the spring length) would normally be required.

6 The Effect of Non-Zero Flexure Clamping Angles.

Figure 6 indicates how the force-displacement characteristic varies with non-zero flexure clamping angles. The lever radius used for all curves is unity (lever radius = spring blade length) and sets of curves for other radii are not shown but are very similar in general appearance. The dashed line is the infinite-radius or equal-springs-in-each-direction line. The central parabolic curve shown in black is for zero clamping angles and is the same as the R=1 curve of figure 5 (with different vertical and horizontal scaling).

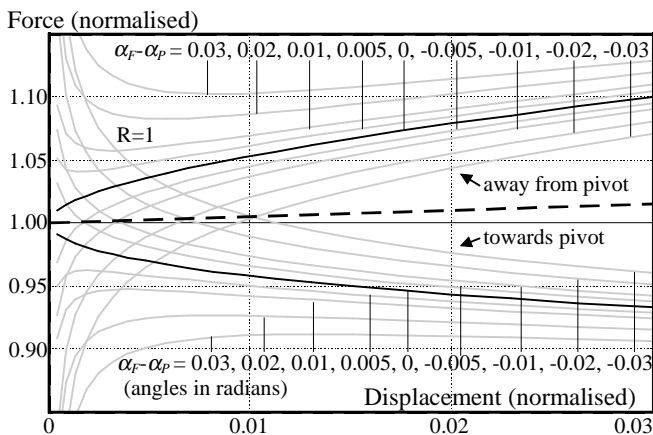


FIGURE 6. Force-displacement dependence on clamping angle.

The grey curves indicate the force-displacement relationship for various non-zero clamping angles. It does not seem to matter which end of the spring is given an offset angle - they both have almost identical effect. In fact if one end is offset to an angle in one direction and the other in the opposite direction (to form a slight “S” when uncompressed), then a curve graphically indistinguishable from the zero angle clamping curve is obtained. For this reason the curves on the plot have been labelled with the difference in clamping angle $\alpha_f - \alpha_p$ because this is the value that counts.

Although not shown, the zero-offset black curves reach unity at almost zero displacement before falling sharply to zero below that. The convex-up grey curves reach zero by gently falling away, while the others reach zero somehow by passing unstably through infinity (in fact the force is quite limited by the compressibility of the neutral axis which is neglected in

this mathematical model). It may be seen that clamping angle offsets which launch the blade towards its main deflection direction “rounds” the left side of the curve, while a launch in the opposite direction to its main deflection “sharpens” it into a rise to infinity (so that the blade wants to “snap-through” to the opposite deflection as it becomes uncompressed).

What is significant in these curves is that if the springs are chosen to predominantly bend towards the pivot (to provide a reduced spring-rate), then the normally unstable section of the curve near zero compression can be ameliorated with a non-zero clamping angle to round the left side of the curve. In fact by choosing the best radius (or in/out bending ratio) together with some clamping angle, it is possible to obtain a spring-rate as low as desired which is also a minimum (force-displacement point of inflection) at the operating point - giving stability above and below. This optimisation will be explored in section 8.

7 Experimental Verification

A bell-crank based isolator stage shown in concept in figure 7a, was built as shown in figure 7b to allow verification of the suspension technique. The suspension arm of the crank was 140mm long and the sprung arm 70mm giving a 2:1 lever ratio. The crank was pivoted with a flexural pivot (Lucas “Free-Flex” 6016-600) to allow friction free pivoting and the clamps for the spring blades were made of brass and are shown in more detail in figure 7c. The clamps were attached with a single bolt allowing clamp angle adjustment and the angle was set with a screw adjustment protruding vertically from the clamping block. Horizontal screws acting on the block allow fine setting of initial buckling, and a motion limit adjustment prevents overstraining.

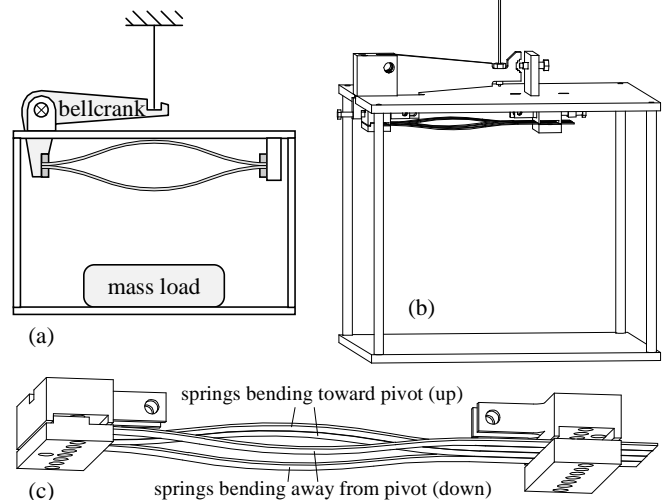


FIGURE 7. (a) Schematic and (b) Drawing of prototype isolator for testing the Euler spring technique. (c) Detail of spring clamping arrangement.

The clamps were fitted with 4 spring blades of unmodified feeler gauge stock 0.635mm thick (0.025”) and 12.7mm wide and clamped tightly with bolts between blades 1 and 2 and between blades 3 and 4. All of the measurements mentioned

in this report were made with a free blade length between clamps of 100mm and with a total loading of approximately 45kg with small amounts of mass being added or removed to obtain force vs displacement measurements. The suspension wire (most readily to hand) was greatly oversized and should contribute an additional spring-rate of 52% of the Euler rate, and the flex pivot another 3.5%. Initially the resonant frequency and Q-factor were measured from a ring-down with two springs up and two down. In theory, taking into account the 2:1 lever ratio and including the additional suspension spring-rates, a resonant frequency of 0.98Hz should be obtained. However a frequency of 1.77Hz was measured with a Q-factor of 50. This Q-factor suggests that if a spring-rate reduction technique was applied, it should be possible to reduce the resonant frequency down to approx 0.25Hz before the Q-factor approaches unity (Q-factor typically varies as frequency squared in this situation).

We also investigated the characteristics of the structure by applying various masses and noting displacements with various spring up/down settings and clamping angles, and measured the resonant frequency at each setting. Two of the 5 data sets are shown. Figure 8 shows the measurements made with clamping angles approximately zero, and figure 9 shows the measurements made with $\alpha_p = -0.023\text{rad}$. For each set a particular mass was applied, and displacement readings taken for the various spring up/down combinations that were stable. The dots at the centre of the short line segments are the force-displacement coordinates while the slope of the line through the dot indicates the gradient found from the measured resonant frequency at that point.

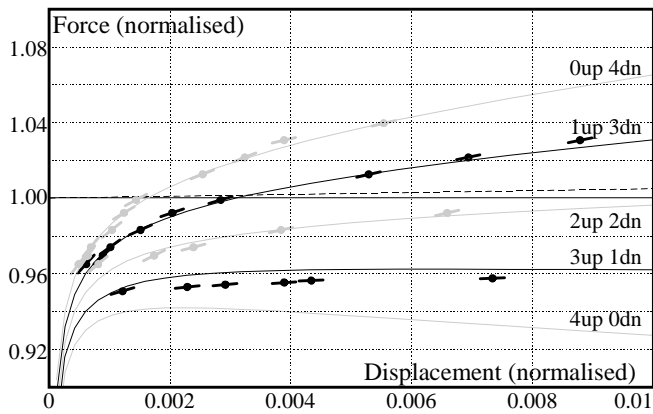


FIGURE 8. Comparison of measured force-displacement with theory.

The continuous lines through the points were obtained by the numerical routines outlined above and lines were plotted for all five possible spring up/down settings even though some were unstable and could not be measured by simply applying mass. The theoretical lines had some parameters that were not exactly known which were adjusted for best fit. Initially these only included the zero displacement and Euler critical load for each graph. However it was not possible to obtain a reasonable fit between the zero offset angle data of figure 8 and the sideways parabolas of figure 5 particularly when the gradients were taken into account. This is obvious by

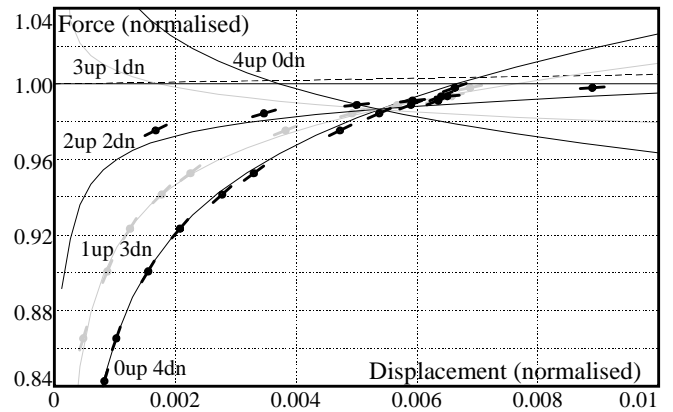


FIGURE 9. Comparison of measured force-displacement with theory.

comparing the gradients of the 2up/2down data against the dashed line which is the approximate force-displacement relation expected for this case.

Our explanation for this obvious departure from theory is that the clamping is non-ideal in that even though the clamping jaws of all blades are at the same angle (being side-by-side between the same jaws) yet it is possible that there is some “slip and stick” effect at the launching edges which allows springs bending in one direction to effectively be launched at a small angle in that direction while blades bending in the opposite direction are launched at a small angle in the opposite direction. Adding a single additional global parameter to account for a small “slip and stick” angle allowed quite good fits to all curves to be obtained. The global fitted value for this angle occurring at both ends of all four springs was 0.0039rad. This small error (in relation to the angles shown in figure 6) results in a spring-rate more than an order of magnitude higher than expected for the 2up/2down case. It was also apparent that this effect had slowly increased with time and usage. Initially the resonant frequency was measured at 1.77, followed by 2Hz when measuring some transfer functions, and finally 3Hz when measuring the effects of clamping angles - and this drift seems to have occurred without the spring clamping being loosened or changed.

We are confident from Britvec’s analysis [1] (2-16) that the non-extensible theory used above is applicable and the theoretical curves obtained are correct. We note that he also found significant departures from theory when measuring fixed-end columns (eg figs 5-4.3 & 5-4.5) whereas his measurements on pin-ended columns (section 3-4) were more in agreement with theory. However due to better clamp design, his departures were small enough to be put down to “imperfections”.

8 Optimising Spring-Rate Cancellation Range

From an examination of figure 6 and its discussion in section 6 it is evident that there exists a unique solution for the lever arm radius and clamping angle offset that will provide a turning point minimum in the spring-rate at some operating

displacement. Of particular interest is this solution for the simplest case which only uses blade spring(s) bending towards the pivot. These solutions are plotted in figure 10.

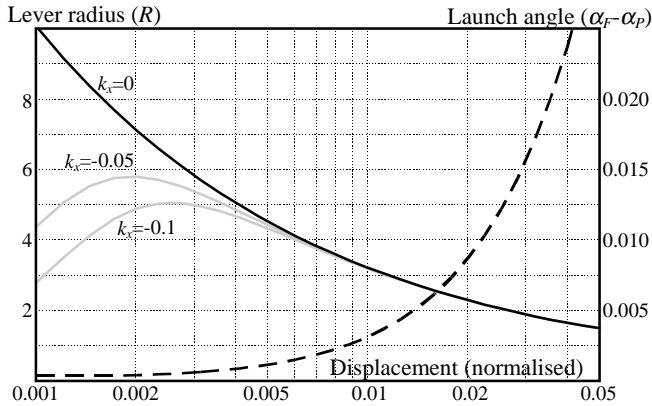


FIGURE 10. Turning point solutions giving radius and launching angles dependent on operating displacement.

The solid lines give the lever radius (as a ratio to blade length) required to obtain a minimum resonant frequency at the operating displacement shown on the x -axis, while the dashed line gives the launch angle required. Since these angles are small and the required value is complicated by the exact boundary conditions such as the difference between clamping and launching angle mentioned in the previous section, this angle needs to be made adjustable. The black lines are the solutions to obtain a zero vertical spring-rate from the combined effects of lever radius and launch angle, while the grey lines are solutions for slightly negative spring-rates to give values of -5% and -10% of the balanced Euler spring-rate $mg/(2l)$. Some small negative value of spring-rate may be desired in order to compensate for the finite spring-rate contribution of pivot and suspension wire bending (see discussion of eq (7)).

It is apparent from figure 10 that the lever radius required for typical displacements in the 0.005 to 0.01 range are quite large and impractical for the simple lever structure shown in figure 1. However using a trapezoidal shaped linkage structure for the lever as shown in figure 11 allows a very long radius to be obtained from short structural elements. The radius is readily preset by choice of the height difference between the front and back blocks of the trapezoid. The launching angle of one end of the spring blades is then finely screw-adjusted to obtain the desired low resonant frequency.

The frequency tuning curves for one particular operating point (Euler spring compressed by 0.65% of its length) have

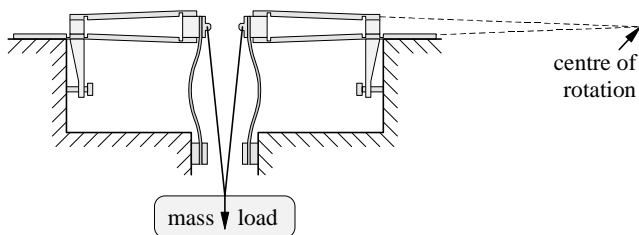


FIGURE 11. Schematic of a reduced spring-rate isolator.

been calculated and are shown in figure 12. The black curve indicates how the resonant frequency varies as a function of displacement for the zero spring-rate solution calculated in figure 10. The grey curves indicate how this curve is approached as the launching angle approaches the correct value for zero frequency, ϵ being the angle away from this correct value. Bearing in mind that the limited Q-factor prevents usefully reducing the resonant frequency below about 0.25 of the unreduced Euler value, it seems that a useable but quite limited working range can be obtained with the resonant frequency only rising to 0.75 of the Euler value.

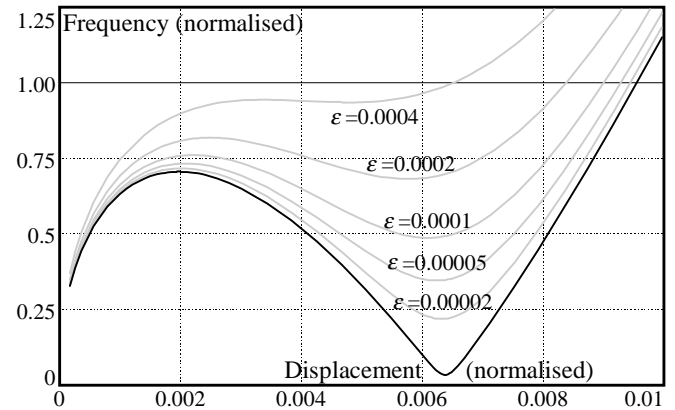


FIGURE 12. Frequency tuning for an operating displacement of 0.0065.

9 Conclusion

The effect of the geometrical parameters on the force-displacement characteristic of a simple lever constrained Euler spring mechanism have been explored by theory and experiment. Apart from the case with equal springs bending towards and away from the pivot (which is almost identical to parallel compression and has an almost straight-line characteristic), the nature of the non-linearities obtained are quite unsuited to spring-rate reduction.

A technique to use the radius and clamp angle effects together has been presented which allows a reduced spring-rate characteristic to be obtained together with a simplified (single-direction) spring arrangement, albeit with a limited working range. Given that the technique is most usefully applied to conditions of constant load and small vibrations, and that spring mass can be reduced (and performance increased) in direct proportion to a reduction in working range[2], this limited range is likely to be acceptable.

Theoretical spring-rates near the buckling knee are not easily obtained without careful clamp design or provision for launch angle adjustment. We might suggest making the clamp jaws from material which is at least as hard as the springs themselves and which has slightly protruding jaw edges to stress the material almost to yield along the launching edges when clamped tight.

Acknowledgment

This work was supported by the Australian Research Council, and is part of the research program of the Australian Consortium for Interferometric Gravitational Astronomy.

References

1. S.J. Britvec, "The stability of elastic systems", New York: Pergamon Press Inc, 1973.
2. J. Winterflood, D.G. Blair, "High performance vibration isolation using springs in Euler column buckling mode", To appear.
3. H.W. Reddick, F.H. Miller , Advanced mathematics for engineers, 2nd ed. Wiley, New York, 1947, Art. 33.
4. *Mathematica* is a registered trade mark of Wolfram Research (<http://www.wolfram.com>).